“Development of a script-based package for analysis of work hardening behaviour”

Abhinav Garg (17118002)

Aman Sharma (17118013)

Supervised by – Dr Sumeet Mishra

DEPARTMENT OF METALLURGICAL AND MATERIALS ENGINEERING

INDIAN INSTITUTE OF TECHNOLOGY ROORKEE

MAY 2021

Table of Contents

1 Introduction

1.1 Background

Often experiments in the field of plasticity require the researcher to know mechanical properties like yield strength, Young's modulus, etc. and get information about the microstructure directly from the tensile experiment dataset. Despite their need in every experiment or analysis, the process of collecting these prerequisites have not been automated and the manual intervention is still needed.

1.2 Motivation

Work hardening analysis of a material forms a foundation of further research in plasticity. So calculation of parameters like yield strength, Young's modules, constants in different plasticity models, etc is a prerequisite before one can proceed with their main objectives. However, all these parameters were calculated semi-manually. For example, software like Origin were used to plot a line parallel elastic region and the intersection point would return the yield strength. The problem lied in finding the intersection point as the huge number of data points made difficult for a naked eye to identify the exact intersection point. Conditions worsened when we rely completely on human beings for calculation. Since these parameters were utterly important, we decided to automate this process which would eventually rectify the above stated example and problems.

1.3 Objective

Given the engineering stress-strain data of an aluminium alloy, create a script which extracts maximum relevant information about the materials. The information which our scripts outputs are as follows.

1. Identify Young's Modulus, Yield Strength, and Ultimate Tensile Strength.
2. Separate the plastic region from the entire plot.
3. Return a work hardening plot give only the plastic region.
4. Fit different dislocation-density based model and compute their parameters.
5. Plot the YLD2000 yield criterion given the strength ratio and r value or values of principal stresses obtained from crystal plasticity models.

1.4 Structure

The report consists of 5 chapters each segregated for a purpose. *Introduction* outlines the introduction by providing a backdrop of work hardening analysis and listing the motivation and objectives behind the report. *Literature Review* elucidates the theory our experiment and reports build upon. *Model Implementation and Results* presents a delineated explanation of our experiments and justifies the insights and results we draw upon. *Conclusion and Future work* concludes our purpose and results of the experiment and finally, *References* ends the report by giving due credit to the authors whose works proved useful for our research in this area.

2 Literature Review

2.1 Stages of Strain hardening

A typical true strain versus true stress curve for a light-weight alloy looks as follows:

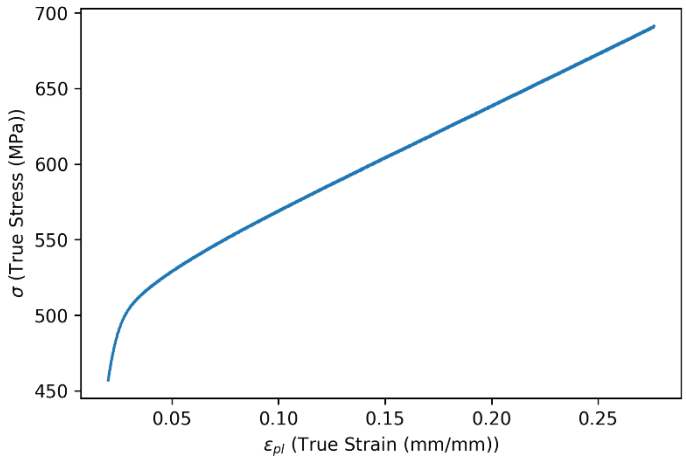

Figure 1 Plot of true strain vs true stress (material: Additive Manufactured SS 316L).

Numerically differentiating the above data yields an important figure which is called a Kocks-Mecking plot. The different stages in the plot below provides a feasible way to understand the microstructural properties.

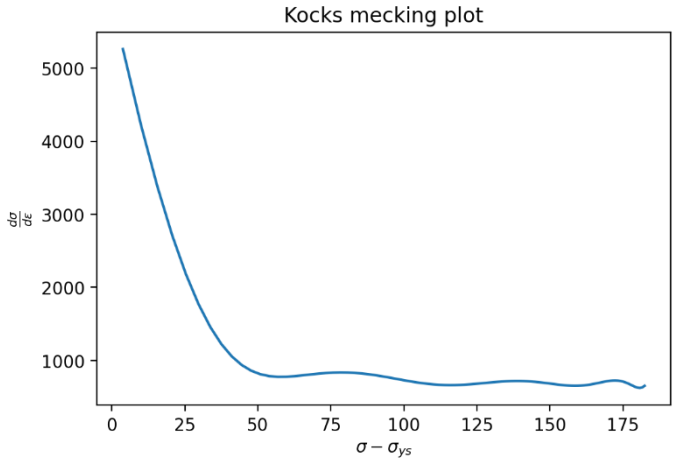

Figure 2 Kocks-Mecking plot (material: Additive Manufactured SS 316L).

Theoretically, five stages [1 pp. 309-311] can be observed in the above plot but practically, especially with a lightweight aluminium alloy, it is not the case. A brief description of each stage is listed down below.

I Low level of hardening in single crystals. As the report focus largely on analysis of polycrystal materials (lightweight aluminum alloys), this stage won't be considered further.

II It corresponds to highest rate of work hardening and can be obtained when the linear part of the graph is extrapolated to intercept the y-axis. That one single intercept represents stage II. The point marks beginning of plastic deformation and the end of elasto-plastic transition.

III This stage can be clearly observed in the above plot. It is the initial linear decrease in work hardening rate as the flow stress increases.

IV Stage III eventually breaks down and the linear decrease converges to an *almost* constant value. This is because the rate of accumulation of dislocations and dynamic recovery become approximately equal. Interpretation of this stage is crucial to study large strain processes such as extrusion and rolling.

V It is very difficult to observe this stage via experiments as it requires attaining very high magnitudes of strain which is not possible in real-life. Theoretically, the flow stress saturates and the work hardening rate becomes almost constant with a very low value.

2.2 Hollomon equation

An elementary approach to find out work hardening behaviour of a material is to fit the experimental data of tensile test experiment in the Hollomon's Equation and then use the parameters obtained to describe the strain hardening behaviour.

$$\sigma = K\varepsilon^n \tag{2.1}$$

Where σ is true stress;
K is strength coefficient;
ε is true strain;
n is work hardening exponent.

One example of fitting is as follows:

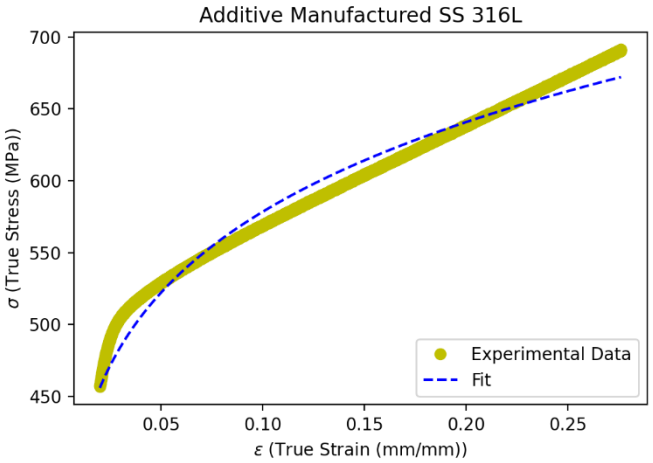

Parameter	Value
K	812.9174 MPa
n	0.15

Figure 3 Fitting Hollomon equation over Additive Manufactured SS 316L data.

The prevalence of this equation and its uses, one of them being determining the value of uniform elongation, which is equal to the work hardening exponent, are quite profound. However, modern research in aluminium and its alloys have discovered few limitations in results concluded from this equation.

1. There are no conditions in this equation which tell about the fracture point and thus, it tends to predict infinite strength for materials being tested.
2. The parameters K and n are not independent of each other. Moreover, they do not provide information about the microstructural relevance which is an important finding for a metallurgist.

Thus, we considered some advanced models for predicting work hardening behaviour. They are described in the upcoming sections.

2.3 Phenomenological modelling: Kocks-Mecking theory

Kocks-Mecking model is an archetype for a dislocation density-based model. It was the first of its kind to relate the internal stresses with the dislocation density. It is able to determine the strength of the material by dislocation-dislocation interaction.

$$\sigma = M\alpha Gb\sqrt{\rho} \tag{2.2}$$

Where σ is true stress;
M is average Taylor factor (usually 3 for polycrystal materials);
α is numerical constant;
G is shear modulus;
b is magnitude of Burgers vector;
ρ is dislocation density

Following this model, the variation of ρ can be derived by considering two concurrent effects in the material – accumulation of dislocation and dynamic recovery [2 p. 73]. The storage is represented in terms of dislocation density, shear strain increment, and the mean free path of dislocations before they were immobile.

$$\frac{d\rho}{d\varepsilon^p} = \frac{M}{bL} \tag{2.3}$$

Dynamic recovery is caused by the annihilation of stored dislocations. This process happens when the dislocation moves from one slip plane to another. More specifically, cross-slips in screw dislocations and climb in the case of edge dislocations. Incorporating this factor in equation (2.3), the evolution of dislocation density can be modelled as:

$$\frac{d\rho}{d\varepsilon^p} = M\left(\frac{1}{bL} - k_2\rho\right) \tag{2.4}$$

Where k_2 is a constant strongly dependent on temperature but weakly dependent on strain rate.

2.4 Coarse grained forest dislocation density-based model

This model is one implementation of the Phenomenological modelling: Kocks-Mecking theory for single phase and coarse-grained materials.

$$\frac{d\rho}{d\varepsilon^p} = M\left(k_1\sqrt{\rho} - k_2\rho\right) \tag{2.5}$$

The constants k_1 and k_2 describe the variations of the concurrent effects described in the above section.

Solving the differential equation after rearranging the equation and substituting (2.2) in the interim equation results in:

$$\sigma = M\alpha Gb\,\frac{k_1}{k_2}\left(1 - e^{\frac{-k_2\varepsilon M}{2}}\right) \tag{2.6}$$

A typical curve modelled using this equation looks like the below figure.

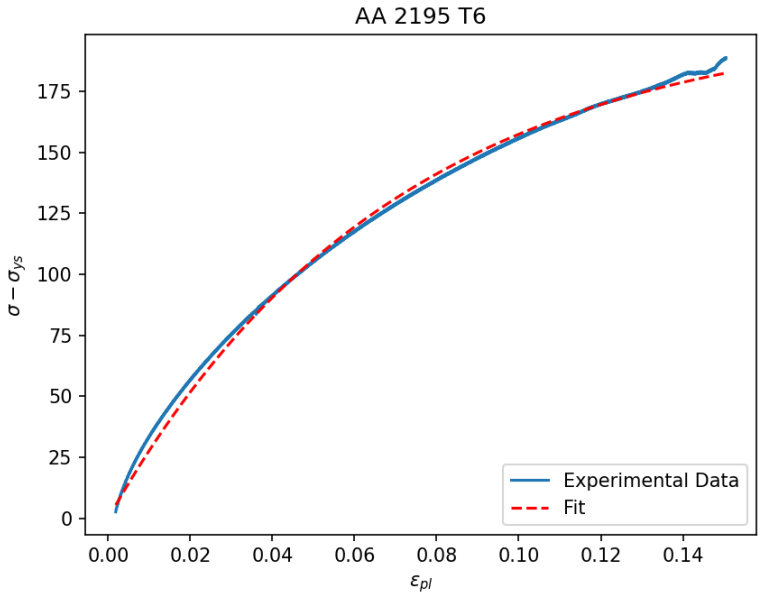

Figure 4 Fitting Kocks-Mecking model (Voce equation) on an experimental data (material: AA 2195 T6).

As one can see from the equation and the plot, the curve, unlike the Hollomon equation, does not predict infinite strength and has a saturation value. Substituting the equation with parameters accounting for saturation stress and work hardening rate, the equation gets transformed to Voce equation.

$$\sigma = \sigma_s \left(1 - e^{\frac{\theta_0}{\sigma_s}\varepsilon_{pl}}\right) \tag{2.7}$$

Where σ_s is saturation stress;

θ_0 is initial work hardening rate (magnitude of work hardening rate in stage II);

ε_{pl} is true plastic strain.

Saturation stress is the maximum amount of dislocation density a material can store. However, reaching this value is practically not possible in the case of tensile testing as necking initiates before one can attain saturation stress.

2.5 Geometric obstacle model

The geometric obstacles in the materials refer to the grains. This model assumes that when the grain size is small enough, the mean free path of the dislocations can be identified using grain diameter (d). In other words, the number of geometric obstacles should outnumber the dislocations. It is assumed that the grain diameter does not change much during the process of tensile deformation.

Accounting for this moderation, we only need to substitute L by d to obtain a new model. The relation between true stress and true plastic strain can further be determined by solving the differential equation. [3]

$$\frac{d\rho}{d\varepsilon^p} = M\left(\frac{1}{bd} - k_2\rho\right) \tag{2.8}$$

$$\sigma = \alpha MGb\sqrt{\frac{k}{k_2}}\sqrt{1 - e^{-Mk_2\varepsilon_{pl}}} \tag{2.9}$$

This model is applied to materials where grain boundary hardening can be observed. Please note that this model is applied for grains of submicron sizes only. Formally, $d < \frac{10}{\sqrt{\rho}}$ should be satisfied for the grain.

2.6 Hybrid model

A more general case (disregarding the assumptions in the above two sections) is to combine the effects of both obstacle types. We can assume that the densities of the obstacles can be superimposed which implies both types of obstacle are equivalent in immobilising the dislocation [2 p. 79]. Thus, the model becomes a combination of equation (2.5) and (2.8).

$$\frac{d\rho}{d\varepsilon^p} = M\left(k + k_1\sqrt{\rho} - k_2\rho\right) \tag{2.10}$$

2.7 Anisotropic yield criterion: Barlat YLD2000 model for plane stress condition

Over the past decades, multiple continuum models for predicting yielding behaviour have been proposed to keep up with the advancement in materials. Criteria like Von Mises [4] accurately predicted the yield locus of an isotropic material. However, it is not applicable to anisotropic materials. An advancement of Von Mises was the family of Hill criteria which incorporated parameters for anisotropic materials, but this model could not properly predict the yielding behavior, especially for Al alloys [5 pp. 22-23]. A contemporary researcher, Hosford, also proposed a non-quadratic model based on Hershey's model [6] which formed the basis for more complex and advanced yield criteria.

$$\emptyset = \emptyset' + \emptyset'' = 2\bar{\sigma}^a \tag{2.11}$$

Where $\emptyset' = |s_1 - s_2|^a$;
$\emptyset'' = |2s_2 + s_1|^a + |2s_1 + s_2|^a$;
a is material constant.

This model was extended by Barlat et *al*. [7] who proposed a series of models accounting for materials exhibiting planar anisotropy. Out of which the most popular was Yld2000-2d. It introduced X$'$ and X$''$ to incorporate for the anisotropy in materials by multiplying the principal stresses with a transformation matrix.

$$\begin{bmatrix} X'_{xx} \\ X'_{yy} \\ X'_{xy} \end{bmatrix} = \begin{bmatrix} C'_{11} & C'_{12} & 0 \\ C'_{21} & C'_{22} & 0 \\ 0 & 0 & C'_{66} \end{bmatrix} \begin{bmatrix} s_{xx} \\ s_{yy} \\ s_{xy} \end{bmatrix} \tag{2.12}$$

$$\begin{bmatrix} X''_{xx} \\ X''_{yy} \\ X''_{xy} \end{bmatrix} = \begin{bmatrix} C''_{11} & C''_{12} & 0 \\ C''_{21} & C''_{22} & 0 \\ 0 & 0 & C''_{66} \end{bmatrix} \begin{bmatrix} s_{xx} \\ s_{yy} \\ s_{xy} \end{bmatrix} \tag{2.13}$$

So, the isotropic functions $\emptyset'$and $\emptyset''$ become:

$$\emptyset' = |X'_1 - X'_2|^a$$

$$\emptyset'' = |2X''_2 + X''_1|^a + |2X''_1 + X''_2|^a \tag{2.14}$$

The principal values of X' and X'' can be computed using the following two equations.

$$X_1 = \frac{1}{2}\left(X_{xx} + X_{yy} + \sqrt{\left(X_{xx} - X_{yy}\right)^2 + 4X_{xy}^2}\right) \quad (2.15)$$

$$X_2 = \frac{1}{2}\left(X_{xx} + X_{yy} - \sqrt{\left(X_{xx} - X_{yy}\right)^2 + 4X_{xy}^2}\right) \quad (2.16)$$

Please note that given the pure tensile nature of our experiments (tests along principal directions), all terms with subscript xy are neglected (their values will be assumed to be 0) and we will not be discussing them further.

Solving equations (2.11), (2.13), (2.15), and (2.16), we get:

$$2\bar{\sigma}^a = \left|s_{xx}(C'_{11} - C'_{21}) + s_{yy}(C'_{12} - C'_{22})\right|^a + \left|s_{xx}(2C''_{21} + C''_{11}) + s_{yy}(2C''_{22} + C''_{12})\right|^a + \left|s_{xx}(2C''_{11} + C''_{21}) + s_{yy}(2C''_{12} + C''_{22})\right|^a \quad (2.17)$$

The values of these transformation coefficients are replaced by anisotropic constant as follows:

$$C'_{11} = \alpha_1$$
$$C'_{22} = \alpha_2$$
$$C'_{21} = C'_{12} = 0 \text{ (only three variables are independent in } C')$$
$$2C''_{21} + C''_{11} = \alpha_3$$
$$2C''_{22} + C''_{12} = 2\alpha_4$$
$$2C''_{11} + C''_{21} = 2\alpha_5$$
$$2C''_{12} + C''_{22} = \alpha_6$$

Plugging the values of the anisotropic parameters into equation (2.17) returns the yield locus of the function. However, before substituting the values, we need to derive their magnitudes. We would need 6 equations to compute the values and they are given by two equations namely – equation for computing yield stress and r value. Further, each equation is solved for 3 stress states – tensile test along rolling direction, tensile test along transverse, and balanced biaxial test. Thus, we get a total of 6 equations. Please note there are two more anisotropic parameters in theory of Yld2000-2d, α_7 and α_8, but we are not considering that as no shear stresses are involved in our experiment.

$$F_i = |\alpha_1\gamma_i - \alpha_2\delta_i|^a + |\alpha_3\gamma_i + 2\alpha_4\delta_i|^a + |2\alpha_5\gamma_i + \alpha_6\delta_i| - 2\sigma_i^a \quad (2.18)$$

$$G_i = (\alpha_1 p_i + \alpha_2 q_i)\,\mathrm{sgn}(\alpha_1\gamma_i - \alpha_2\delta_i)\,|\alpha_1\gamma_i - \alpha_2\delta_i|^{a-1} + (\alpha_3 p_i - 2\alpha_4 q_i)\,\mathrm{sgn}(\alpha_3\gamma_i + 2\alpha_4\delta_i)\,|\alpha_3\gamma_i + 2\alpha_4\delta_i|^{a-1} + (2\alpha_5 p_i - \alpha_6 q_i)\,\mathrm{sgn}(2\alpha_5\gamma_i + \alpha_6\delta_i)\,|2\alpha_5\gamma_i + \alpha_6\delta_i|^{a-1} \quad (2.19)$$

Index i	Mode	γ	δ	σ	p	q
1	Rolling (0°)	$\frac{2}{3}$	$\frac{-1}{3}$	σ_0	$1 - R_0$	$2 + R_0$
2	Transverse (90°)	$\frac{-1}{3}$	$\frac{2}{3}$	σ_{90}	$2 + R_{90}$	$1 - R_{90}$
3	Balanced biaxial	$\frac{-1}{3}$	$\frac{-1}{3}$	σ_b	$1 + 2R_b$	$2 + R_b$

Table 1 Constants needed to compute the anisotropic parameters.

Solving the system of 6 linear equations above using the implementation of modified Powell method [8] in SciPy [9], yield the anisotropic parameters from α_1 to α_6. This will be delineated more when we discuss the implementation below.

A typical yield criterion curve obtained from this model looks like below.

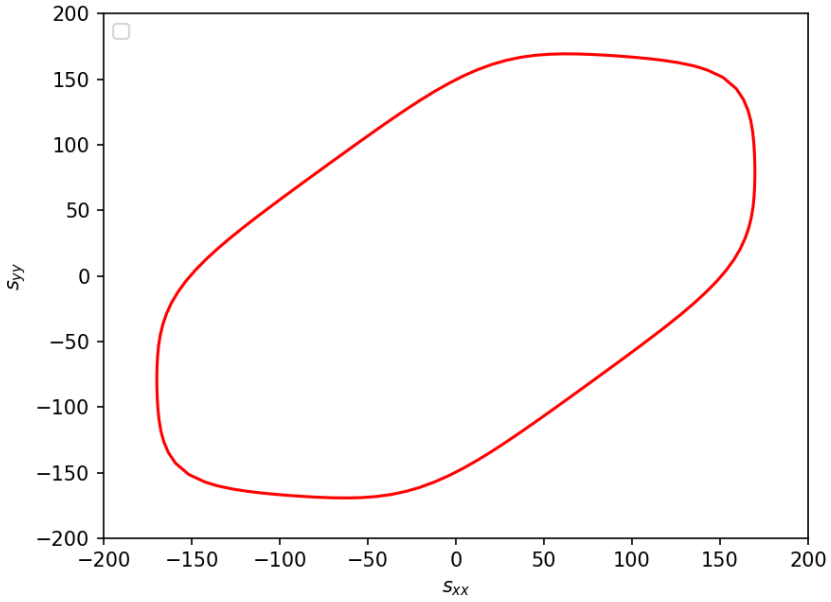

Figure 5 Typical YLD2000 plot generated using random principal stresses.

The anisotropic parameters for this curve were taken from the works by Basak and Panda [10]. Table IV in reference [10] summarises the anisotropic parameters for different pre-strain. However, we used the case where no pre-strain was applied. As one can observe YLD2000 is a more generalised case of yield criterion. Earlier models such a Von Mises' criterion was a specialised case of YLD2000 because if we put all the anisotropic (α_1 to α_6) constants equal to each other and the material constant as 2, we get a locus of Von Mises' criterion.

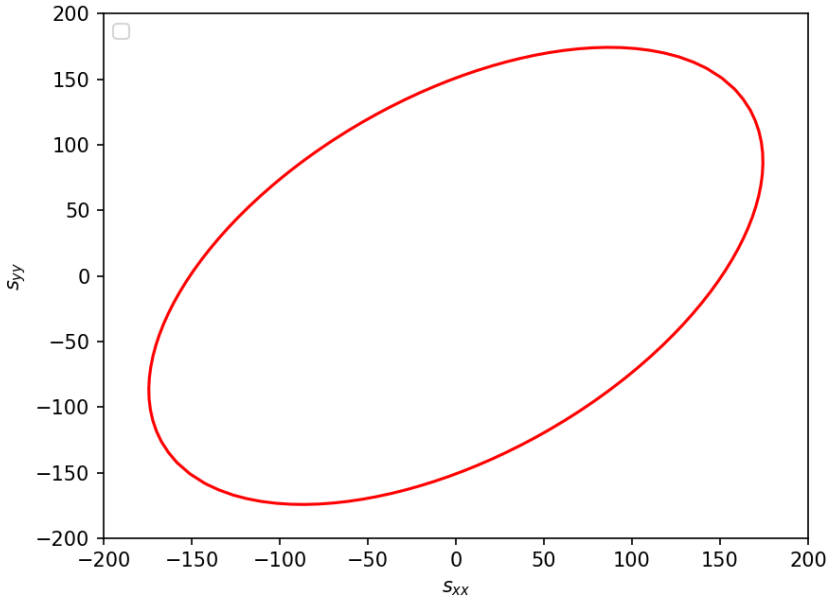

Figure 6 Data is similar to what in Figure 5 except a=2 and all anisotropic parameters are set to 1.

Similarly, had we put the material constant as 1, the curve would replicate the locus obtained from Tresca criterion.

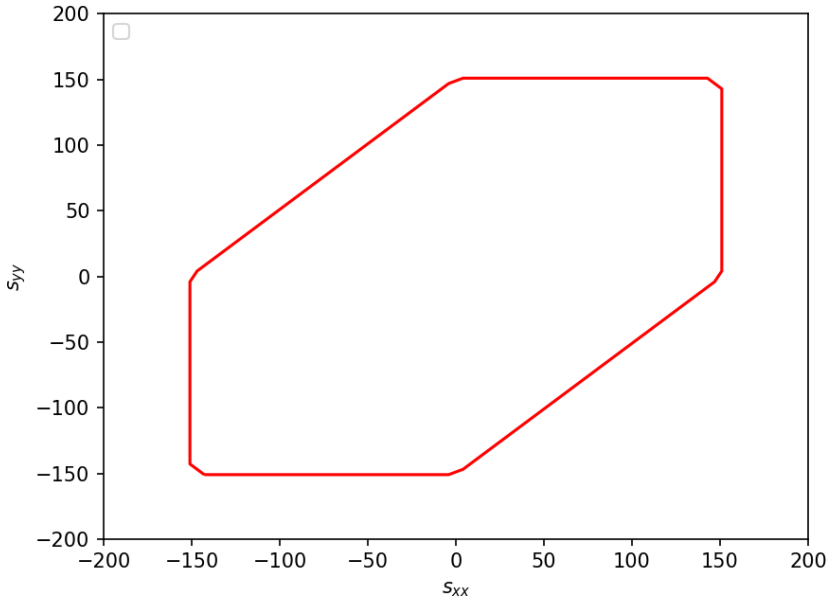

Figure 7 Data is similar to what in Figure 5 except a=1 and all anisotropic parameters are set to 1.

3 Model Implementation and Results

3.1 Jupyter notebook script

The implementation of all the models above has been written using Jupyter notebook scripts and all of them have been hosted on GitHub as a repository [11]. The setup instructions to get the project up and running are delineated in the README attached with the same repository.

The repository follows monolithic structure as it contains all the Jupyter notebooks at one place. The entry point of the notebook is `dataset_initialisation.ipynb`. It takes all the initial input of datasets from the user. Purpose of each notebook is described below.

1. `dataset_initialisation.ipynb` – Takes in the datasets (filters out the negative values of engineering strain and corresponding engineering strain) required for further computation. It also setups up other files and directories to store the output returned from the execution of script.
2. `engineering_strain_stress.ipynb` – Sanitises the input in two steps:
    a. Makes sure there is exactly one engineering stress for every engineering strain.
    b. Smoothens the curve using convolution method implemented in NumPy [12].

    After sanitisation, the script proceeds to solve for Young's Modulus, Yield Strength, and Ultimate Tensile Strength. These parameters help in identifying the plastic region.
3. `true_strain_stress.ipynb` – Computes true strain/true plastic strain versus true stress curve and saves their datapoints.
4. `hollomon_curves.ipynb` – Plots the Hollomon equation and helps in analysis for stages of work hardening.
5. `work_hardening_analysis.ipynb` – Implements various models of work hardening listed in section "Literature Review".
6. `YLD2000.ipynb` – Implements the theory in section "Anisotropic yield criterion: Barlat YLD2000 model for plane stress condition".
7. `utilities.ipynb` – Contains the utility functions for sanitising input, computing, and managing output, etc. used throughout the notebooks.

3.2 Importing stress-strain data

As mentioned above, `dataset_initialisation.ipynb` takes path to the datasets as a python list. Each dataset should be a CSV file and it should follow a format consisting of fixed number of columns and delimiter.

Column 1	Engineering strain	mm
Column 2	Engineering stress	MPa
Delimiter	,	

Table 2 CSV format of dataset.

For example,

```
1E-05,0.05602
1E-05,0.11128
2E-05,0.21463
3E-05,0.44231
```

Inside this notebook, under the heading *Dataset*, there is a python list which takes in **1 or more** paths to various datasets following the above format. Some functions in the script will show a combined plot of the datasets passed whereas some will show each of them individually.

3.3 Finding Young's Modulus, Yield Strength, Ultimate Tensile Strength and extracting the data between YS and UTS

The parameters listed in the heading above were necessary to determine the plastic region of the plot and then eventually performing work hardening analysis over the plots. We devised algorithms to compute them based on heuristics.

3.3.1 Calculation of Young's Modulus

Young's modulus is a mechanical property which determines the stiffness of a solid material in the elastic region. It can be obtained graphically using the plot of engineering strain versus engineering stress by calculating the slope of the line in the elastic region.

To solve this programmatically, we present the user with the below plot and ask them to guess the value of engineering strain and stress up to which the plot seems to be in elastic region.

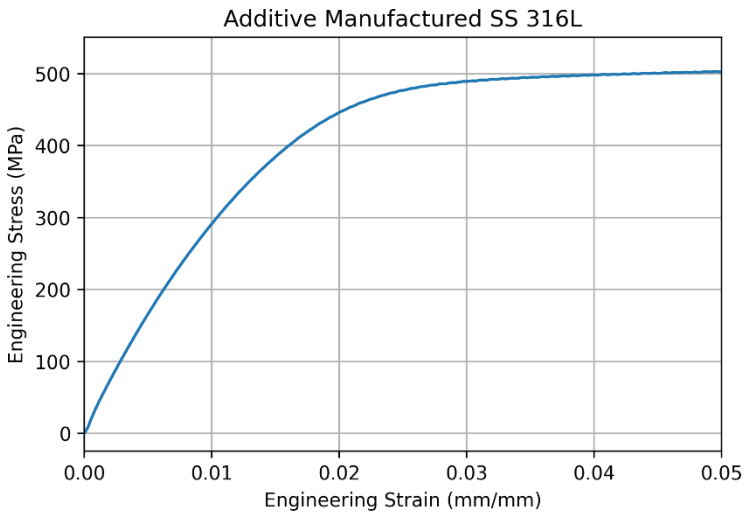

Figure 8 Plot for users to guess the linear region.

After supplying the values, we have implemented a function, `find_nearest`, which tries to find the index of the data point in the original dataset which is closest to the guessed value coordinate. Please note that the coordinate here is a tuple of engineering strain and engineering stress.

Once the data point is found, we fit a linear line from first point in dataset to the computed datapoint using linear regression [13].

For example, an educated guess for the above plot would be 0.015 and $400MPa$ engineering strain and stress, respectively. Accordingly, our script computes the Young's modulus and plots it.

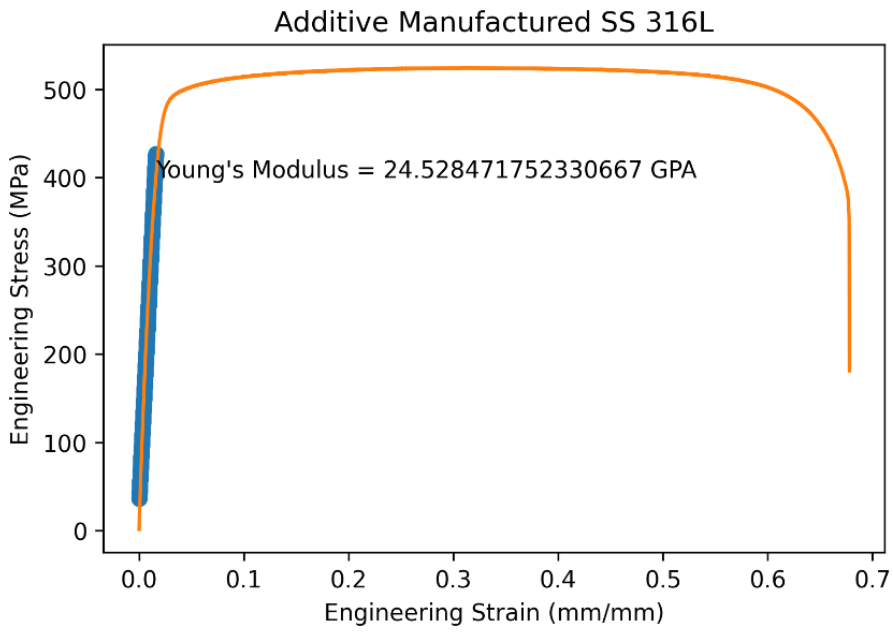

Figure 9 Computed Young's modulus from guessed values.

Please note that since this computation is based on heuristics, the guess cannot be very off. We expect the user using this script to have an idea about the linear region of engineering strain versus engineering stress curve and can approximate where does this region end.

3.3.2 Calculation of Yield Strength

An approximate value of yield strength can be computed by finding out the intersection between a line with slope equal to young's modulus and x-intercept as 0.2% strain and the engineering stress-strain curve.

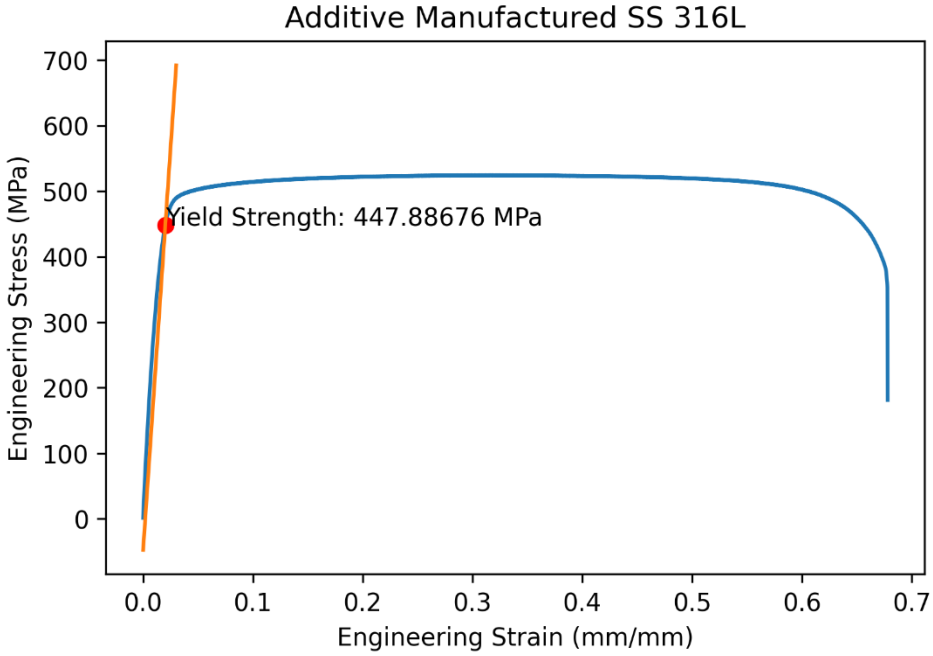

Figure 10 Yield strength based on Young's modulus calculated above.

3.3.3 Calculation of Ultimate Tensile Strength

Ultimate tensile strength is the maximum stress a material can withstand before breaking. Following this definition, we simply calculate the maximum value of engineering stress in the dataset.

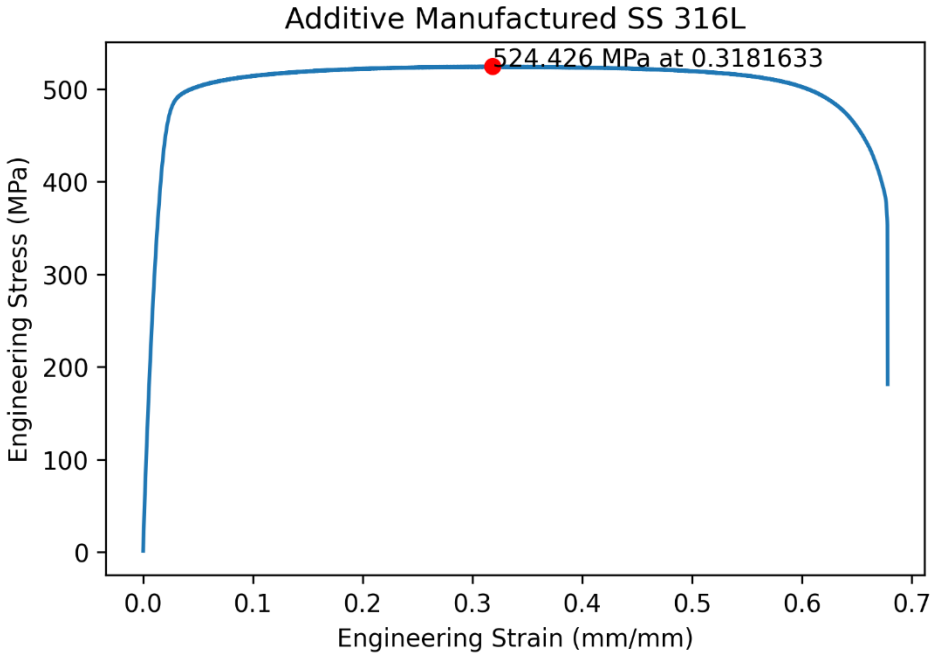

Figure 11 UTS calculation.

We feel that there is scope of an error in this approach but practically, it is negligible if the data acquisition rate of the experiment is in the order of milliseconds.

3.3.4 Plastic region

The elastic region ends at yield strength and the plastic region begins. It continues till the ultimate tensile strength. Thus, the region between the yield strength and ultimate tensile strength will be the focus of our further analysis.

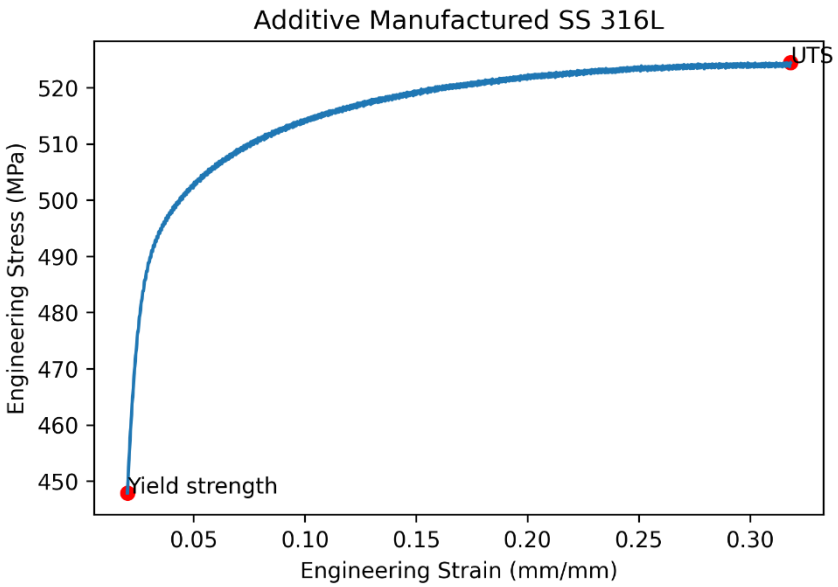

Figure 12 Plot of plastic region.

3.4 Analysis of plastic region

True strain and true stress can be obtained from equations (3.1) and (3.2) which are a function of engineering strain and stress.

$$\varepsilon_{true} = \ln\left(1 + \varepsilon_{engineering}\right) \tag{3.1}$$

$$\sigma_{true} = \sigma_{engineering}\left(1 + \varepsilon_{engineering}\right) \tag{3.2}$$

Applying these equations to the datasets under analysis using NumPy [12], we obtained the variation of true stress with true strain for the materials under consideration.

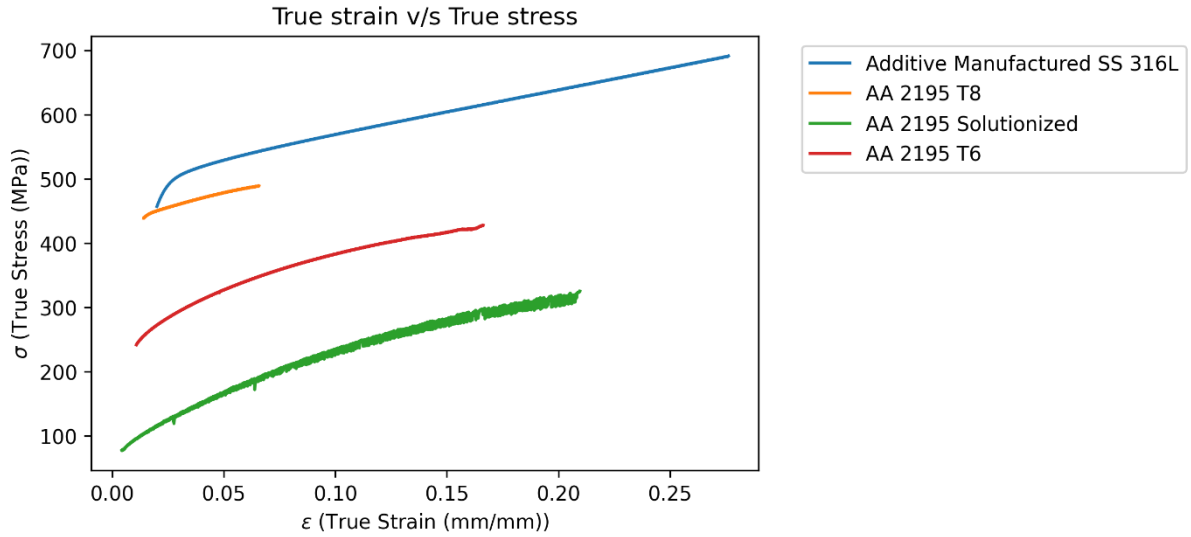

Figure 13 Comparison of true stress-strain for various Al alloys and additive manufactured SS 316L.

Additive Manufactured SS 316L has the highest yield strength due the high initial dislocation density. It has been reported in the literature that additive manufactured samples have high

dislocation density. Additive manufactured samples also have the low angle cell boundaries which contribute towards higher uniform elongation.

AA 2195 T8 is in peak aged condition. As a result, the microstructure can be characterised by the presence of coherent/semi-coherent precipitates, which tend to get sheared by the mobile dislocations. As a result, the overall strain hardening is low for the AA 2195-T8 sample.

AA 2195 Sol is in solution treated condition, where the solute atoms such as Cu and Li are completely dissolved in the Al matrix. The solute elements tend to segregate near the stacking fault. As a result, the stacking fault energy is reduced, which in turn reduces the cross-slip probability. As a result, dislocation annihilation would be sluggish, and more dislocations would be stored in the material. Therefore, the strain hardening is also good for solution treated samples.

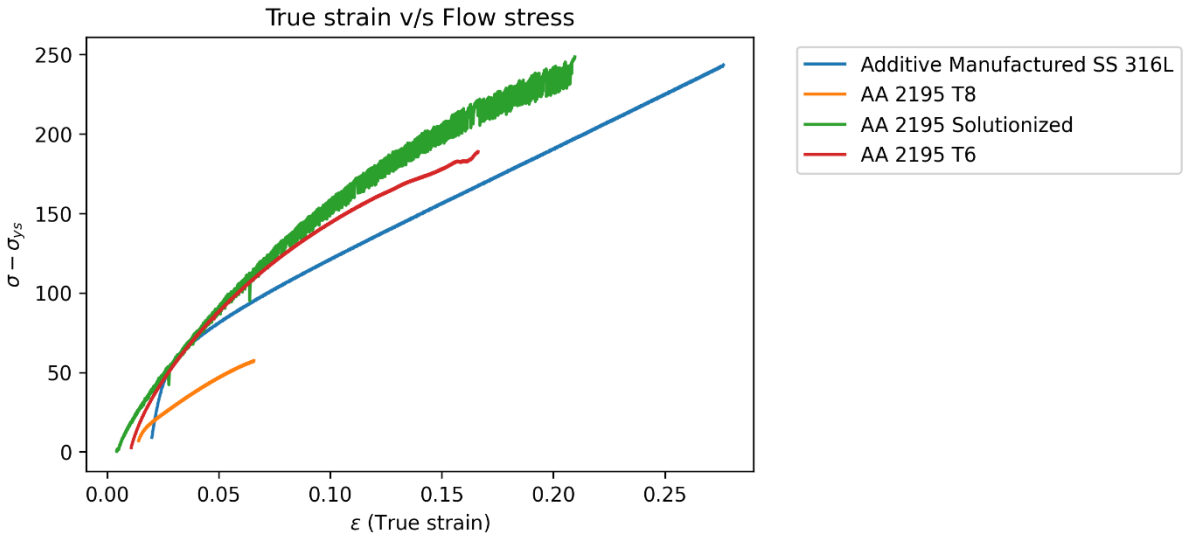

Figure 14 Comparison of flow stress variation with true strain for various Al alloys and additive manufactured SS 316L.

The term *flow stress* is defined which signifies the instantaneous amount of stress required to continue plastic deformation of a material.

$$\sigma_f = \sigma_{true} - \sigma_{ys} \tag{3.3}$$

In practice, initial values of flow stress should be close to 0 for accurate results. However, if they are not, the error can be attributed to excessive machine elongation during tensile testing. One should ensure that their apparatus is stiff and there is no slipping between the grips and specimen.

3.5 $\frac{d\sigma}{d\varepsilon}$ versus flow stress plots

$\frac{d\sigma}{d\varepsilon}$ v/s $\sigma - \sigma_{ys}$ plots, due to their direct practical application, have a special name – *Kock-Mecking plot*. The relate work hardening rate with the flow stress which helps in analysis in two main ways.

1. Its influence on formability, particularly for annealed and solution treated tempers.

2. Controlling the strength in strain hardened tempers for high strain processes such as extrusion, rolling, etc.

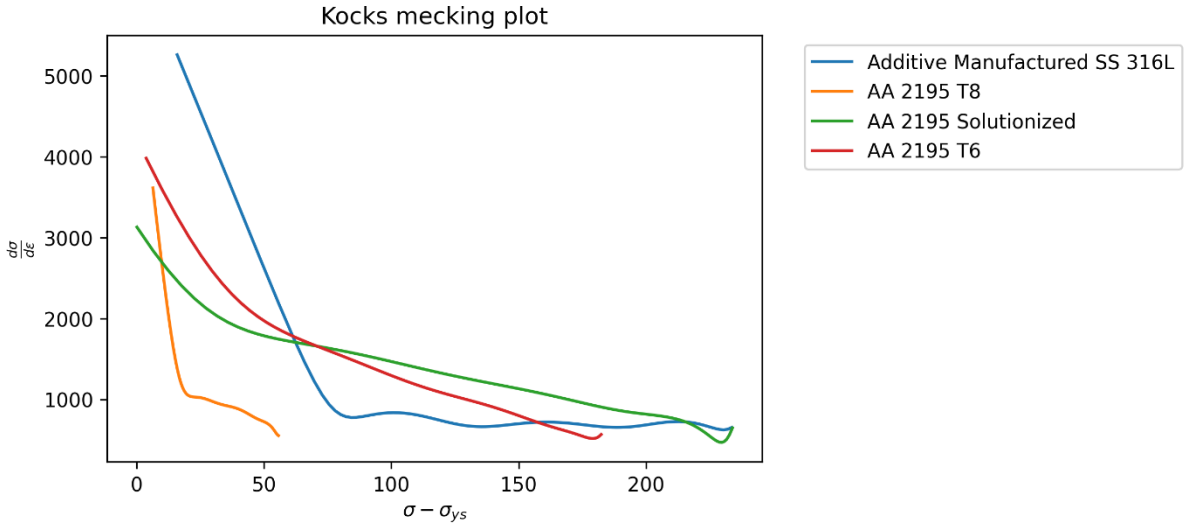

Figure 15 Kocks-Mecking plot for various Al alloys and additive manufactured SS 316L.

The work hardening rate obtained above was differentiated with our own custom function. We calculate the pairwise difference of true strain and true stress and divided them to get the derivative of the dataset. More formally,

$$\frac{d\sigma}{d\varepsilon} = \frac{\sigma_2 - \sigma_1}{\varepsilon_2 - \varepsilon_1}, \frac{\sigma_3 - \sigma_2}{\varepsilon_3 - \varepsilon_2}, \frac{\sigma_4 - \sigma_3}{\varepsilon_4 - \varepsilon_3} \dots \frac{\sigma_n - \sigma_{n-1}}{\varepsilon_n - \varepsilon_{n-1}} \tag{3.4}$$

Where n is the length of the dataset.

Equation (3.4) returns a list of derivates for each true strain and true stress computed before. Note that we will end up with $n - 1$ derivates if originally, we have n points in our dataset of true strain versus true stress plot. We can justify the correctness of this method as the n for our experiments was significantly large so the derivates computed are quite accurate according to the first principle of differentiation.

3.6 Simulating stress-strain curves using various density-based models

We simulated stress-strain curves using various models we have described above. We observed shortcomings in the earlier models which were overcome by the later models as described in next sub-sections.

3.6.1 Forest dislocation density-based model

Forest density-based dislocation model is an implementation of the Voce equation as described in Coarse grained forest dislocation density-based model. So, we tried fitting true stress-strain curves on Voce equation using Levenberg-Marquardt [14] method implemented in SciPy [9] to obtain parameters - θ_0 and σ_s.

The experimental data we obtained in tensile test of AA 2195 T6 was a good fit for this model as shown in Figure 4. However, for materials Additive Manufactured SS 316L and AA 2195 T8, this model was not yielding a good fit, so we tried using different models for these materials.

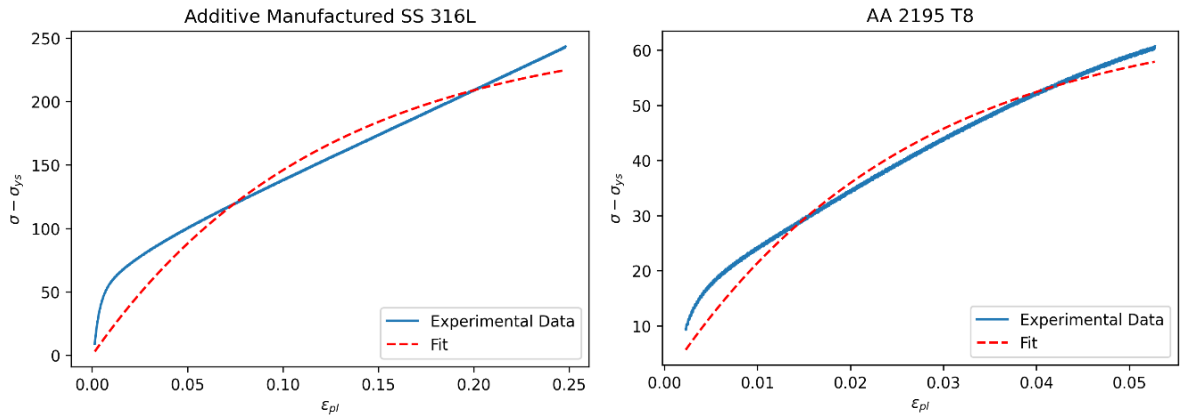

Figure 16 Inaccurate fitting of Voce equation.

3.6.2 Geometric obstacle model

Since this model is sensitive towards its parameters, k and k_2, we wrote script which would allow its user to simulate parameters and see the best fit for themselves. As one can observe here that geometric model fit better for this material compared to Voce equation in Figure 16.

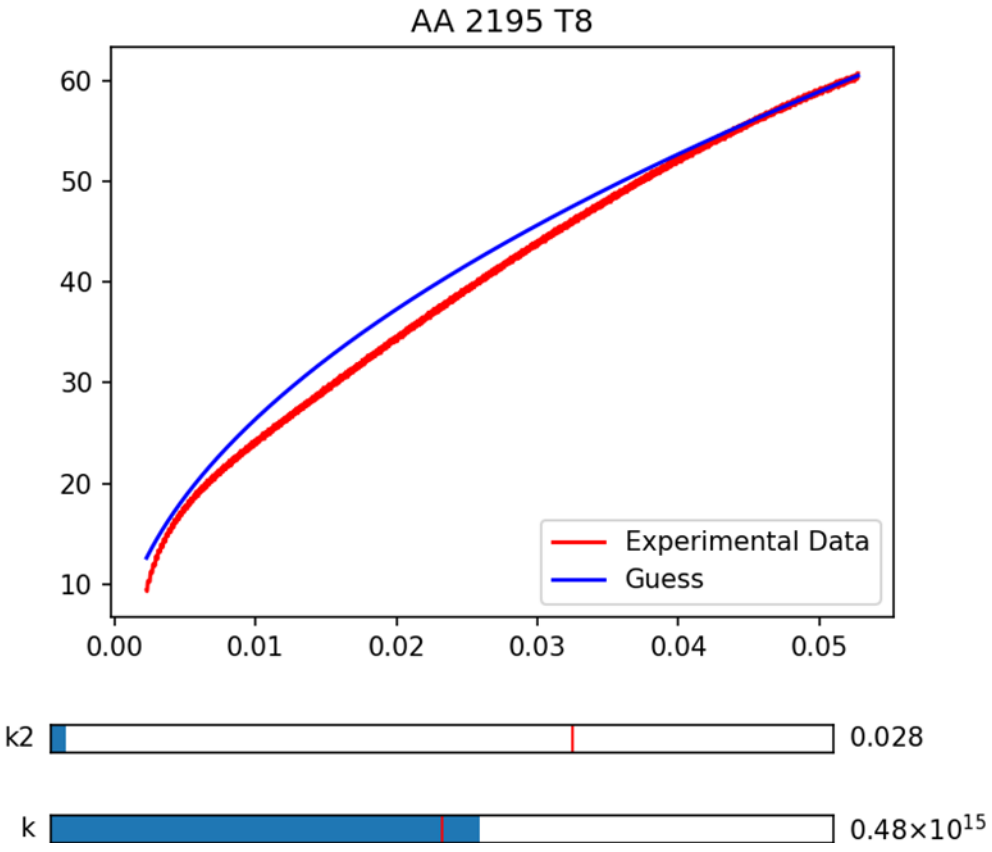

Figure 17 Fitting geometric model on T8 alloy data.

The initial guess, denoted by the red vertical marker in the slider, should be an educated guess. For example, the value of k_2 usually lies between 0.1 and 5, so guessing a value of the order

of 10^5 will yield poor results. Here our initial guesses were 10^{14} and 1 for k and k_2 respectively.

3.6.3 Hybrid Model

This model consists of three parameters – k, k_1, and k_2 which implies that the educated guess now, compared to the above model, has to be more accurate. The differential equation thus formed using these parameters was although solvable, but it was computationally expensive. So we decided to use a method of numerical integration called Runge-Kutta Method [15] which we implemented in the `work_hardening_analysis.ipynb` – Implements various models of work hardening listed in section notebook itself.

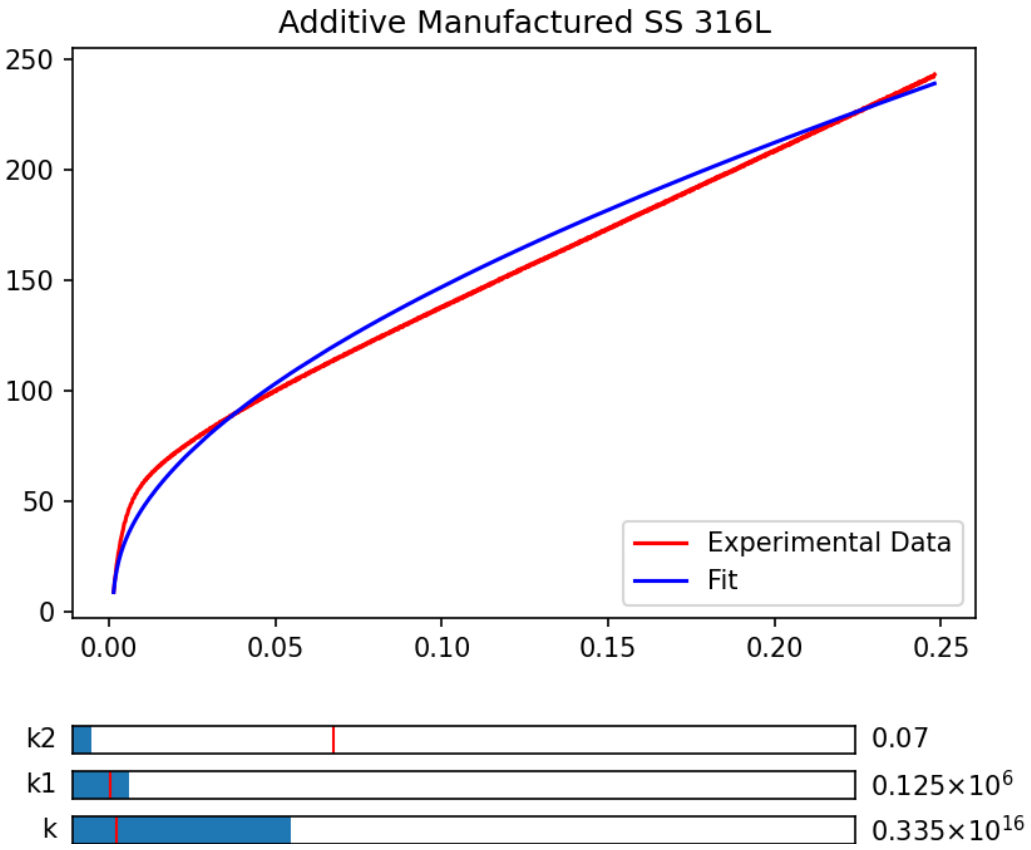

Figure 18 Fitting hybrid model on additive manufactured SS 316L.

With a greater number of parameters, and provided one inputs *educated guesses*, it possible to fit models which were not fitting well in Voce equation as shown in Figure 16.

3.7 Implementation of YLD2000

The notebook `YLD2000.ipynb` – Implements the theory in section "Anisotropic yield criterion: Barlat YLD2000 model for plane stress condition". contains the entire implementation of the model. We first tried to find a typical plot using this yield criteria by generating dummy data of s_{xx} and s_{yy} using `np.linspace` [12].

```
alpha = np.array([1.0021, 1.0849, 1.1022, 0.9761, 0.9681, 0.9770, 1.0482, 0.961])
sxx = np.linspace(-200,200,50)
syy = np.linspace(-200,200,50)
a = 8 # For FCC materials
```

Feeding the above data in equation (2.17), we get a typical YLD2000 plot as show in Figure 5.

One can also obtain the data for s_{xx} and s_{yy} using crystal plasticity modelling. However, an experimentally advanced model like YLD 2000 gives a smoother curve as the curve is of continuum nature. Although solving for the anisotropic parameters is a computationally expensive task, but once it is computed for a material, it is quite feasible to plot the yield criterion at any direction with respect to the rolling direction.

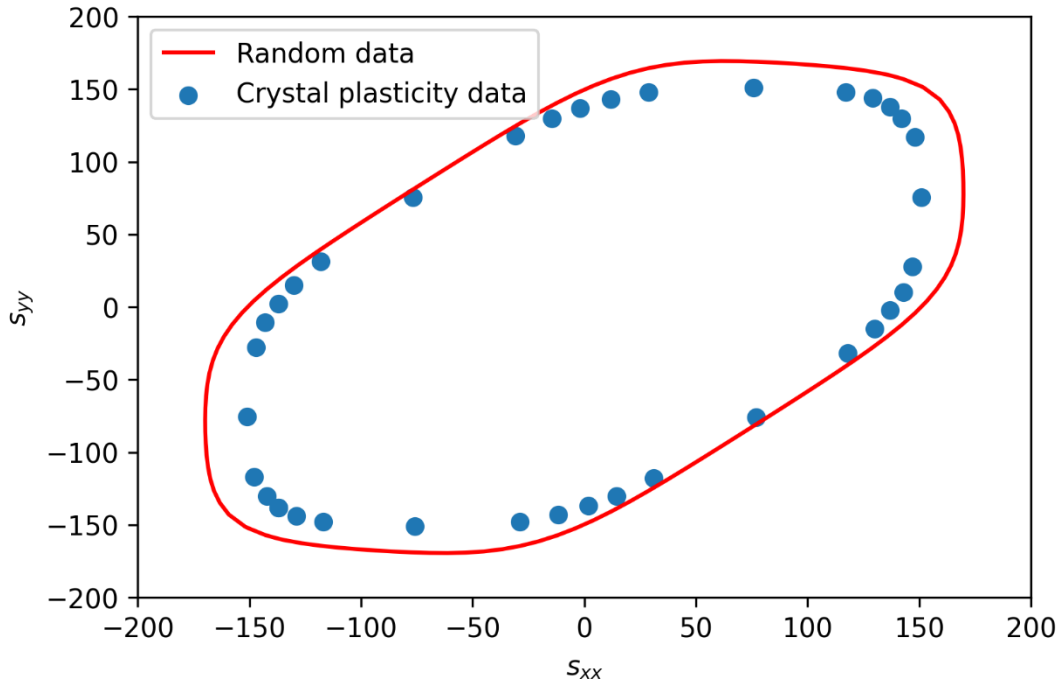

Figure 19 Comparison between random data and crystal plasticity data.

However, to get more practical values of s_{xx} and s_{yy}, we needed to compute the anisotropic parameters, and prior to that the r value (plastic strain ratio) and strength ratio across rolling, transverse, and balanced biaxial direction. The technique to calculate these prerequisites have already been proposed in the works of Basak and Panda [10].

YLD2000 model made computation of yield criteria quite feasible as prior to this model, experimentally advanced crystal plasticity models were used which were computationally expensive. However, the calculation of the anisotropic parameters in YLD2000 model is a challenge but once they are computed for a material, one can easily plot the yield criterion.

Mat.	Strain Cond.	α_1		α_2		α_3		α_4		α_5		α_6	
		Exp	Act	Exp	Act	Exp	Act	Exp	Act	Exp	Act	Exp	Act
EDD	As-rec	1.0021	**1.0208**	1.0848	**1.0586**	1.1022	**1.1295**	0.9761	**0.9770**	0.9681	**0.9684**	0.9770	**0.9939**

	15% EBP	1.0179	**0.9770**	1.0014	**1.0782**	1.0299	**1.0618**	0.9781	**1.0009**	0.9806	**0.9987**	0.9623	**1.0286**
	10% EBP	0.9669	**1.0248**	1.0843	**1.0076**	1.0030	**1.1124**	0.9877	**0.9902**	0.9845	**0.9894**	0.9569	**1.0208**

Table 3 Comparison of our outputs with results in [10].

3.8 Graphical significance of anisotropic parameters

We tried tweaking the anisotropic parameters to find out which section of the curve the parameter is most relevant to. A delta value of 0.1 seemed appropriate to us we observed that the values of these parameters usually lie within $(0.8, 1.2)$.

The dotted line in the following curves represent the original value taken from an article [10 p. 298]. Next, we added and subtracted 0.1 from the dotted curve to obtain the blue and red lines respectively which represent the tweaked curve for the altered parameter.

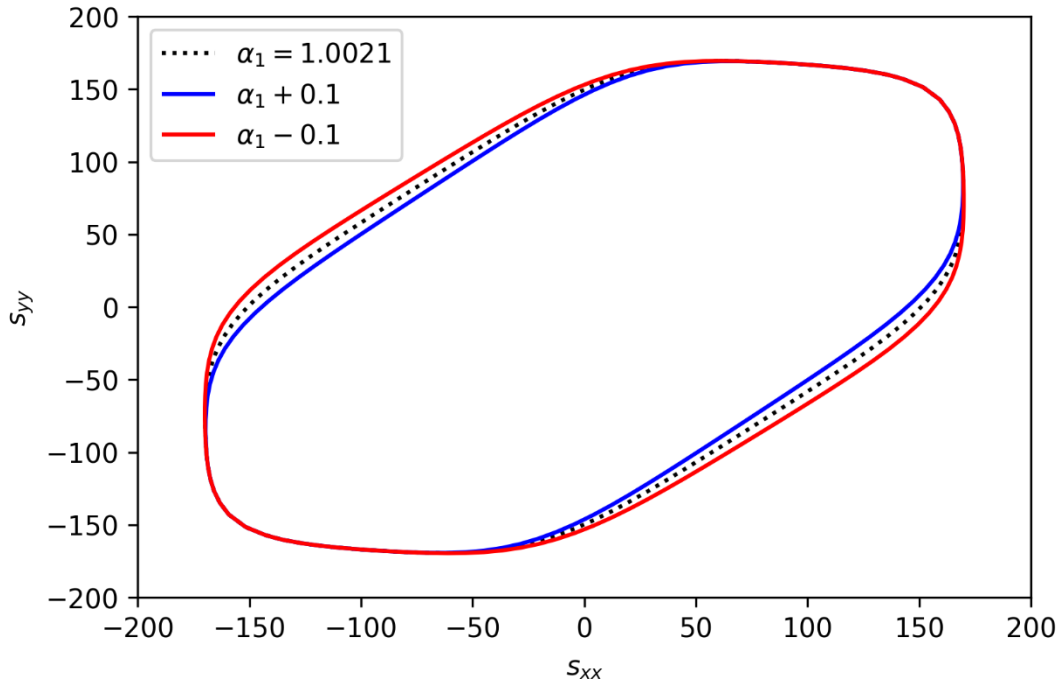

Figure 20 Plot variation when α_1 is increased or decreased.

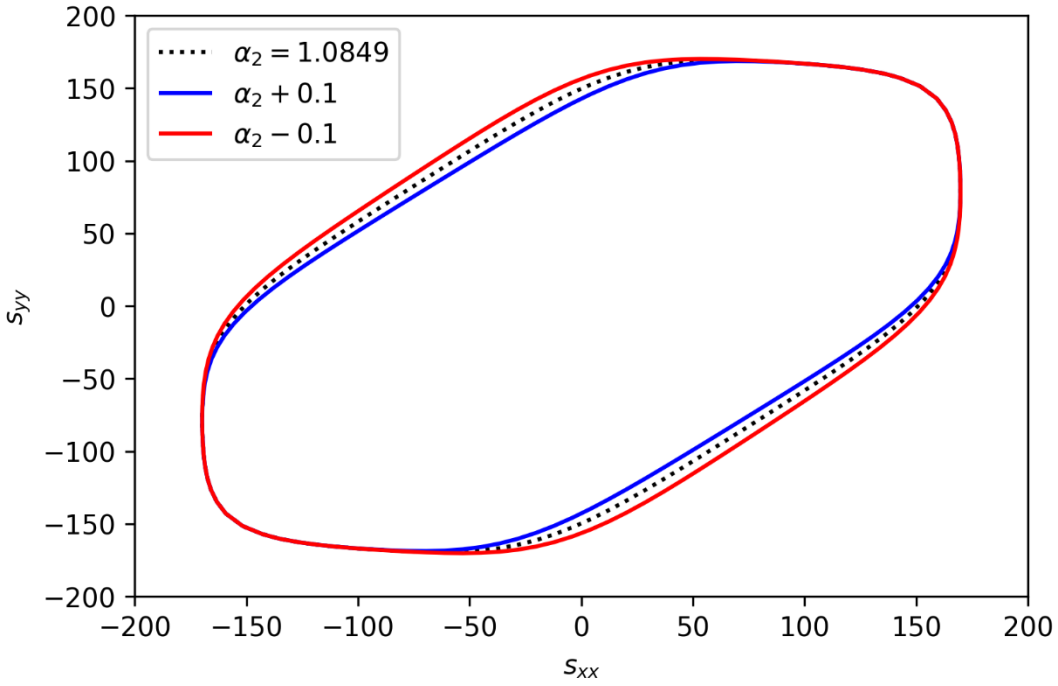

Figure 21 Plot variation when α_2 is increased or decreased.

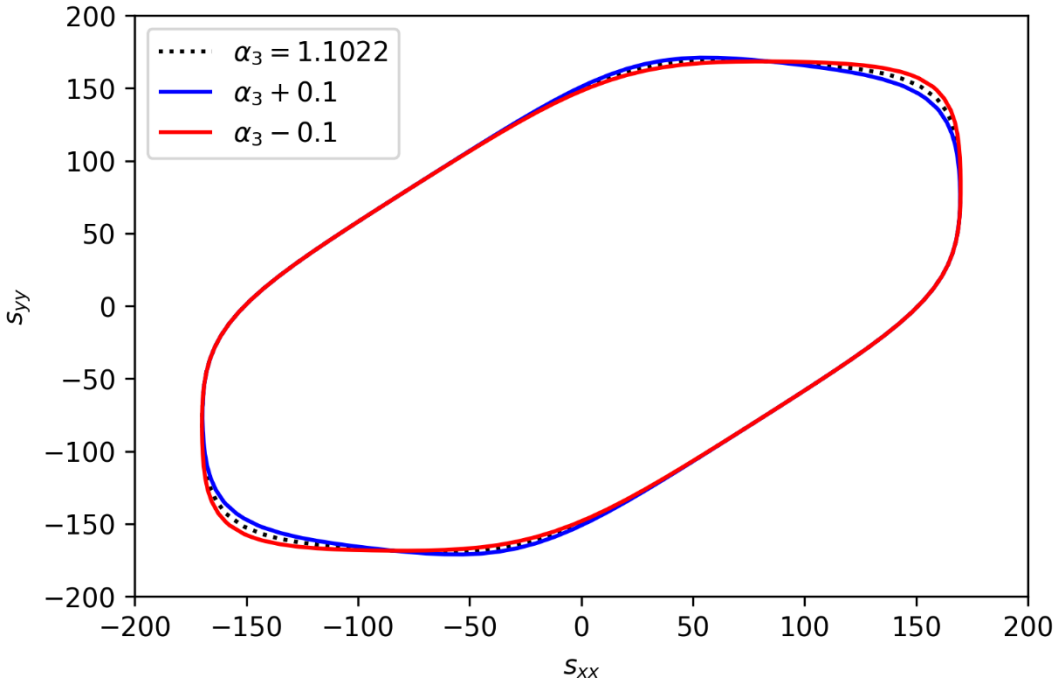

Figure 22 Plot variation when α_3 is increased or decreased.

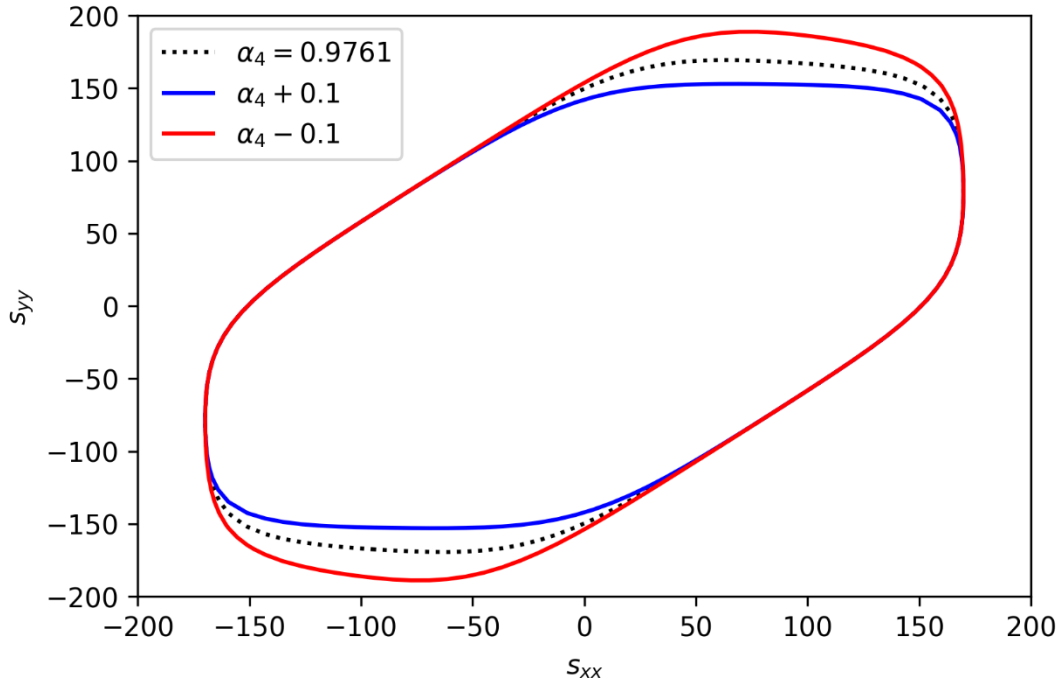

Figure 23 Plot variation when α_4 is increased or decreased.

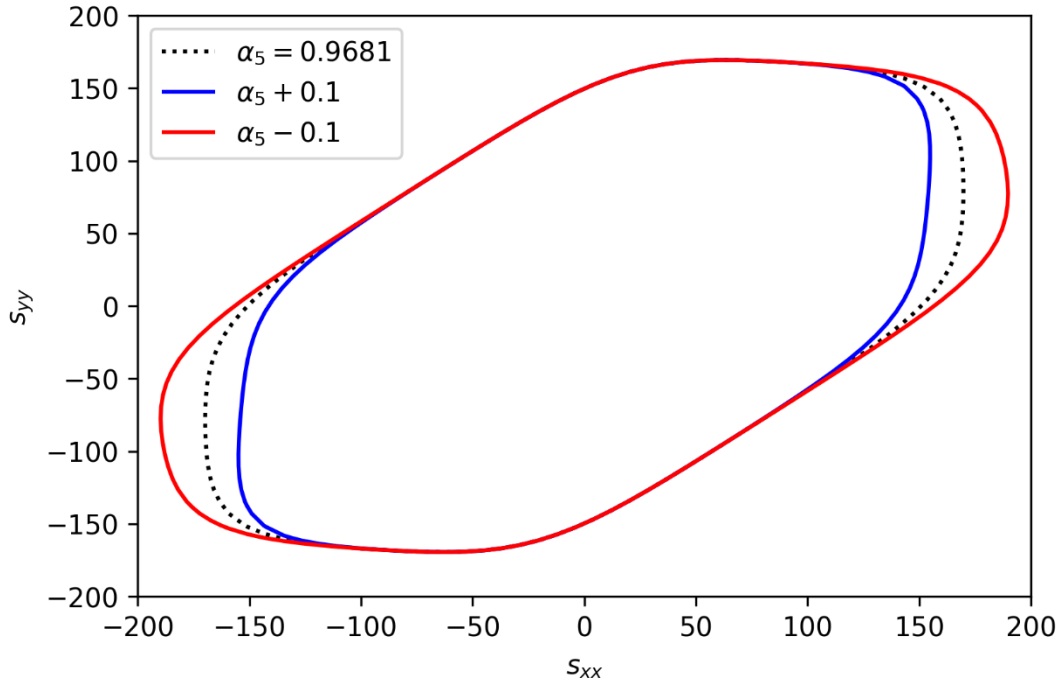

Figure 24 Plot variation when α_5 is increased or decreased.

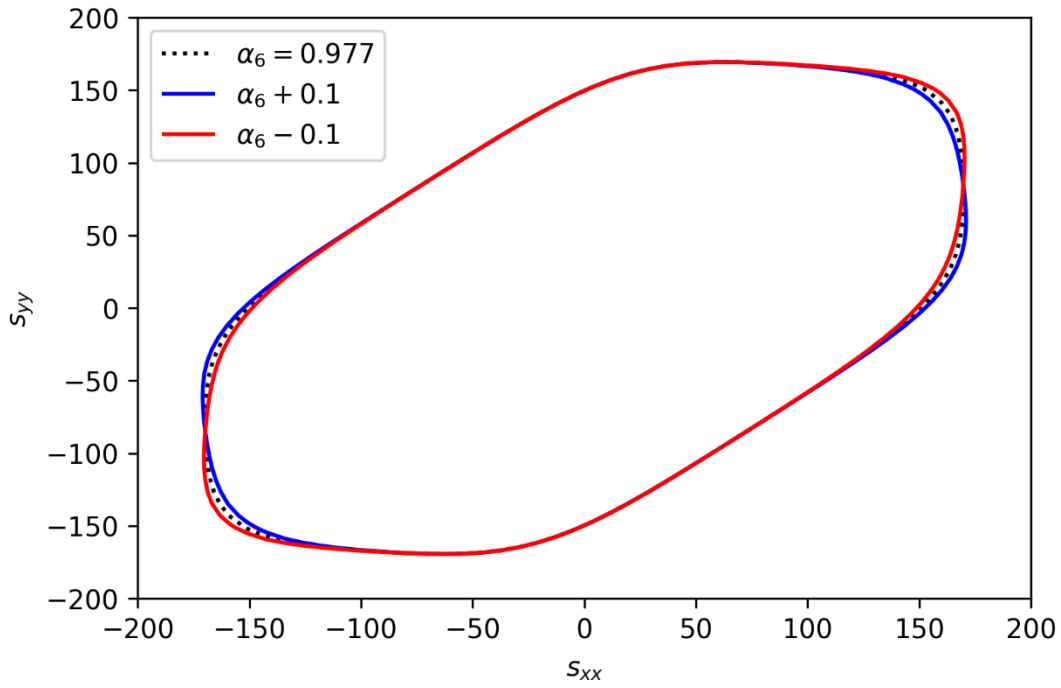

Figure 25 Plot variation when α_6 is increased or decreased.

It can be observed from the above plots that altering α_1 and α_2 majorly influences the region of pure shear in the plot. Modifying α_3 and α_6 affects the balanced biaxial region. α_4 and α_5 are parameters which majorly influences the plane strain along y and x axis respectively. Thus, these two anisotropic parameters will further help the most in plotting the formability limit diagram.

4 Conclusion and Future work

The Python script successfully fulfils the objective of our experiments and automates calculation of the said parameters. All functions written in the script are pure in nature, meaning they always give the same output for the same input. This implies that one will always get the same set of output for the same dataset provided. The only human intervention required is when the script is computing Young's Modulus and asks for the user to input an educated guess. Although the guess may vary, we have written the underlying functions so that the error can be minimised to an extent where it can be considered negligible.

Our work lays a foundation for further analysis of materials. The parameters we have computed are enough to plot a formability limit diagram which has a very high industrial relevance. Apart from addition of more features, there are few improvements which can be made to the current script. We track them in the GitHub repository [11] under the *Issues* tab.

5 References

[1] **Poole, W.J., Embury, J.D. and Lloyd, D.J.** Chapter 11: Work hardening in aluminium alloys. [book auth.] Roger Lumley. *Fundamentals of Aluminium Metallurgy: Production, Processing and Applications.* s.l. : Woodhead Publishing, 2011.

[2] **Estrin, Yuri.** Chapter 2: Dislocation-Density-Related Constitutive Modeling. [book auth.] A.S. Krausz and K. Krausz. *Unified Constitutive Laws of Plastic Deformation.* 1996.

[3] *Analysis of Structural Factors That Control Necking.* **Malygin, G. A.** 2005, Physics of the Solid State, Vol. 47, pp. 246-251.

[4] *Mechanik der plastischen Formänderung von Kristallen.* **Mises, R.V.** June 1928, Journal of Applied Mathematics and Mechanics.

[5] **Alharthi, Hamzah Abdulrahman.** *Accurate Descriptions of the Anisotropic.* 2016.

[6] *The plasticity of an isotropic aggregate of anisotropic face centred cubic* . **Hershey.** 1954, Journal of Applied Mathematics and Mechanics, pp. 241-249.

[7] *Plane stress yield function for aluminum alloy sheets-part 1: theory.* **Barlat, F., et al.** 19, 2003, International Journal of Plasticity, pp. 1297-1319.

[8] *An efficient method for finding the minimum of a function of several variables without calculating derivatives.* **Powell, M. J. D.** 2, 1964, The Computer Journal, Vol. 7, pp. 155-162.

[9] **community, The SciPy.** Optimization and root finding. *SciPy.* [Online] SciPy.org.

[10] *Necking and fracture limit analyses of different pre-strained sheet materials.* **Basak, Shamik and Panda, Kumar Sushanta.** 267, 2019, Journal of Materials Processing Tech., pp. 289-307.

[11] **Sharma, Aman, et al.** Repository for analysing work hardening behavior. *GitHub repository.* [Online] https://github.com/algomaster99/meta-btp.

[12] *Array programming with NumPy.* **Harris, C. R. and Millman, K. Jarrod.** s.l. : Springer Science and Business Media (LLC), September 2020, Nature, Vol. 585, pp. 357–362.

[13] *statsmodels.regression.linear_model.OLS.* **Seabold, Skipper and Perktold, Josef.** 2010. Proceedings of the 9th Python in Science Conference.

[14] **Weisstein, Eric W.** Levenberg-Marquardt Method. *MathWorld.* [Online] https://mathworld.wolfram.com/Levenberg-MarquardtMethod.html.

[15] **Wikipedia contributors.** Runge–Kutta methods. *Wikipedia: The Free Encyclopedia.* [Online] https://en.wikipedia.org/wiki/Runge%E2%80%93Kutta_methods.

[16] **Marshall, Graeme, et al.** Orowan Bowing. *Internet Archive | Wayback Machine.* [Online] https://web.archive.org/web/20110928085736/http://aluminium.matter.org.uk/content/html/eng/default.asp?catid=71&pageid=1006363262.